Transformer-Induced Low-Frequency Oscillations in the Series-Resonant Converter

Hans W. Klesser and J. Ben Klaassens

***Abstract*—The article demonstrates the existence of a number of modes of transformer-induced low-frequency oscillations (TLO's) which can be observed in the series-resonant power converter with a transformer in the resonant circuit, operating under conditions of cyclic stability. The TLO phenomena are mathematically analyzed and the conditions of existence are determined. Experimental observations confirm the outcomes of the mathematical analyses. The critical aspects of the TLO phenomena with respect to the converter performance are explored.**

Introduction

OVER the last decade great interest have been shown in the more sophisticated methods of power conditioning by using resonant circuits for the control and transfer of electrical energy. Numerous papers have been presented on the characteristics of this class of power conversion systems [1], [2].

Natural current commutation of the semiconductor switches is obtained by the use of a single series-resonant circuit. This resonant conversion technique leads to an efficient operation at high frequencies (10 $\cdots$ 100 kHz and more) in combination with low stress in the active switching devices because of the avoidance of switching losses.

The resonant circuit will generate a train of bipolar, quasi-sinusoidal current pulses. This carrier is controlled by a pulse modulation process which will vary the time between two successive current pulses [5].

A demodulation process mechanized by a conventional diode-rectifier bridge will form a unipolar current. An output capacitor will eliminate the ac components in the output current through the dc-load.

The theoretical maximum value of the average output voltage U_o with respect to the source voltage E_s will be limited to $U_{o\max}/E_s = 1$. To overcome this limitation a transformer has to be placed in the resonant circuit. The transformer is used for voltage or current scaling. It also provides galvanic insulation between two networks such as input and output circuits.

The characteristic of the transformer may interfere with the resonant oscillation in the power circuit and may lead to the generation of low frequency oscillations in the resonant circuit of purely a magnetizing current which ultimately can influence the power transfer capacity.

The generation of such a transformer-induced low-frequency oscillation (TLO) is modeled in [4]. This reference did not completely include in the modeling the role of the transformer magnetizing current. Only a single mode of the TLO was considered, resulting in the misleading conclusion that a series-resonant converter using a lossless transformer can not be operated under conditions of cyclic stability for a normalized output voltage $q > 0.5$.

The model presented below includes fully the role of the magnetizing current and evaluates the generation of all possile modes of TLO's, leading to the conclusion that stable operation of the dc-dc series-resonant converter with lossless transformer will be possible for any value of the conversion ratio $0 \leq q \leq 1$.

Principles of Operation

A simplified schematic of the power circuits of the series-resonant converter is shown in Fig. 1.

Its mode of operation consists of the alternate closing of the switching pairs Th11, Th22 and Th12, Th21 and the associated antiparallel diodes $D11$, $D22$ and $D21$, $D22$.

An alternating current i_1 is generated in the components L_1, C_1 and the primary windings of the transformer, the active switching elements, and the input filter capacitor C_s [1], [2].

The average value $|i_1|_{av}$ of i_1 is related to the load current $I_o = |i_2|_{av}$ by

$$I_o = |i_1|_{av} N_2/N_1 \tag{1}$$

where N_i is the number of turns of the relevant winding W_i of the power transformer XF ($i = 1, 2$) and i_2 is the current in winding W_2 of the transformer XF. To simplify the presentation the winding ratio N_2/N_1 is chosen to be one.

Fig. 2 is obtained from figure 1 by representing the transformer in a equivalent circuit diagram by a constant magnetizing inductance L_m.

The leakage inductance is thought to be linked up with the series inductance L_1. Nonlinear effects are assumed to be negligible. All other components are assumed to be ideal.

Fig. 3(a)–(g) show the various switching configurations according to the switches selected in the converter

Manuscript received July 23, 1986, revised July 16, 1987.

The authors are with the Laboratory for Power Electronics, Delft University of Technology, Mekelweg 4, 2628 CD Delft, The Netherlands.

IEEE Log Number 9100528.

0885-8993/91/0700-0326$01.00 © 1991 IEEE

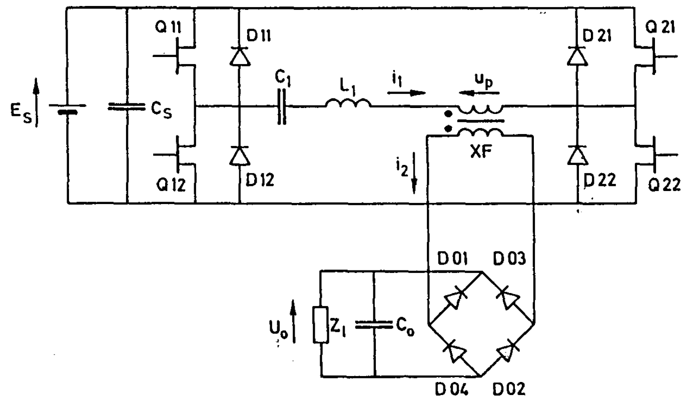

Fig. 1. Circuit diagram of full bridge configuration of series-resonant dc-dc converter.

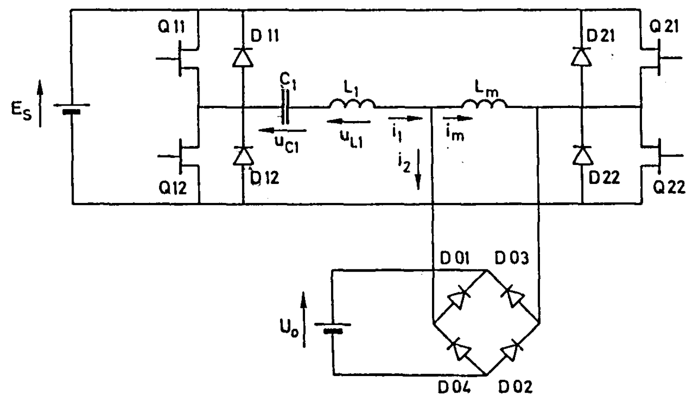

Fig. 2. Simplified schematic of full bridge configuration of series-resonant converter.

network, in which the resonant circuit can be connected to the dc-voltage sources E_s and U_o. TLO waveforms of the resonant current i_1 are generated in the configurations depicted in Fig. 3(f) and (g). These configurations will be arranged at the moment that the resonant current i_1 equals the magnetizing current i_m under the condition that the absolute value of the (primary) transformer voltage u_p is smaller than the voltage U_o on the filter capacitor C_o, so that the rectifier consequently becomes inactive and the resonant circuit is decoupled from the voltage source U_o.

Any of the network configurations of Fig. 3 can be described mathematically by the set of relations (2), provided that appropriate choices are made of the ternary variables j and k:

$$\begin{aligned} jE_s &= u_{C1} + u_{L1} + u_p \\ i_1 &= C_1 du_{C1}/dt \\ u_{L1} &= L_1 di_1/dt \\ u_p &= (1 - k^2)L_m di_1/dt + kU_o \\ j, k &\propto [1, 0, -1]. \end{aligned} \tag{2}$$

Clearly, the second order network configurations displayed in Fig. 3(a)–(d) will generate sine waves with radial frequency

$$\omega_0 = =1/\sqrt{L_1 C_1} \tag{3}$$

while the configurations displayed in Fig. 3(f) and (g) generate sine waves of radial frequency

$$\omega_m = 1/\sqrt{(L_1 + L_m)C_1} < \omega_0. \tag{4}$$

Two examples of a complete cycle of the current i_1 that can be generated by the converter under the condition of cyclic stability are plotted in Figs. 4 and 5 against normalized time

$$x = \omega_0 t. \tag{5}$$

The synthesized sine wave segments which are the construction elements of a more complex current i_1, are encircled, following the sequences *a-f-c-g* and *a-f-e-c-g-e*, indicating that the cycles are generated by switching through the corresponding network configurations of Fig. 3.

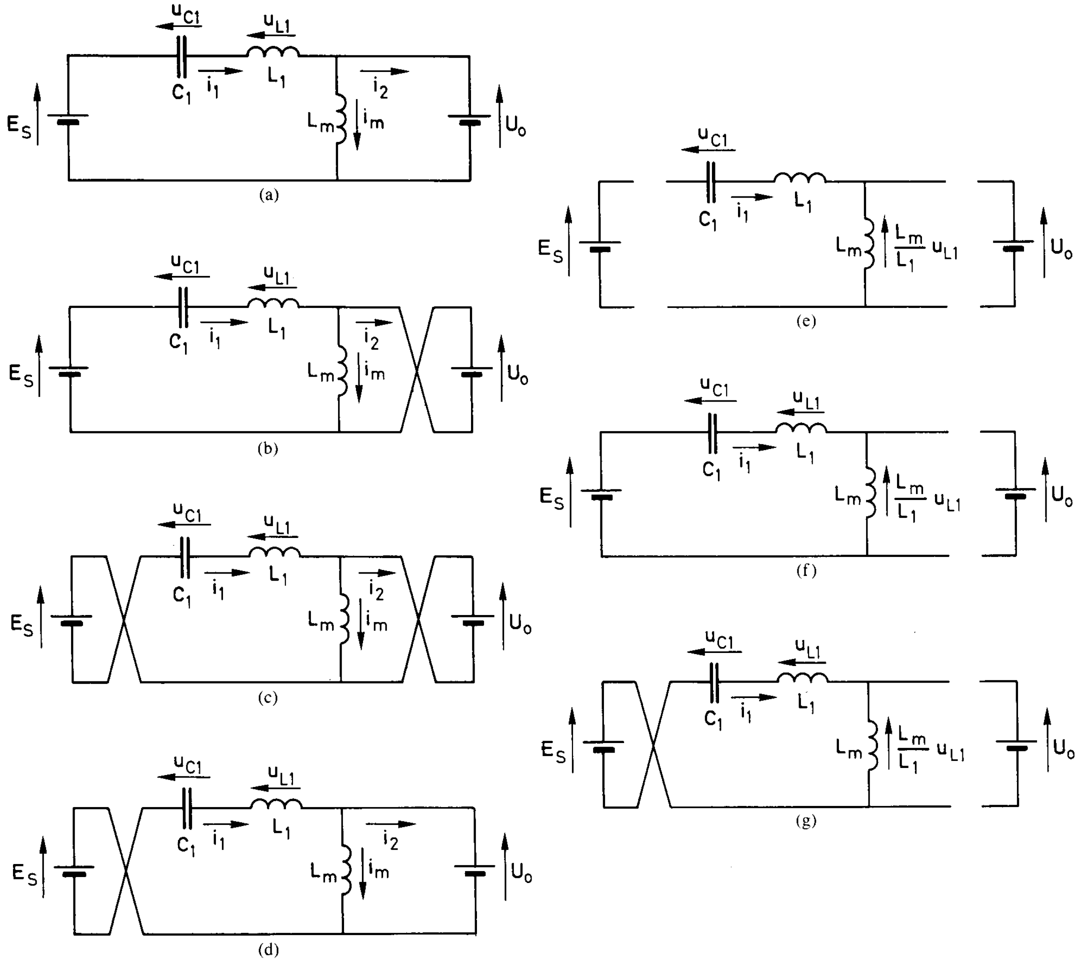

Fig. 3. Equivalent network presentations of Fig. 2. according to appropriate choices of variables j and k in (2): network a: $j = 1$, $k = 1$ (active semiconductors Th11, Th22, $D01$ and $D02$); network b: $j = 1$, $k = -1$ (active semiconductors $D11$, $D22$, $D03$ and $D04$); network c: $j = -1$, $k = -1$ (active semiconductors Th21, Th12, $D03$ and $D04$); network d: $j = -1$, $k = 1$ (active semiconductors $D21$, $D12$, $D01$ and $D02$); network e: $j = 0$, $k = 0$ (active semiconductors none); network f: $j = 1$, $k = 0$ (active semiconductors Th11, Th22 or $D11$, $D22$); network g: $j = -1$, $k = 0$ (active semiconductors Th21, Th12 or $D21$, $D12$).

Both cycles incorporate segments of TLO waveforms f and g, while the cycle shown in Fig. 4 also displays a zero current segment e. In the case of the latter it is said that the cycle has been generated in a mode of discontinuous current operation of the converter. It is noted that the ratio of the length of a TLO sine wave period versus that of a non-TLO sine wave is given by the factor ξ as defined by

$$\xi = \sqrt{(L_1 + L_m)/L_1}. \tag{6}$$

Modes of Operation

Four different modes of discontinuous current operation can occur under conditions of cyclic stability as will be shown below.

One of these has already been displayed in Fig. 5. Half cycles of the other three modes are depicted in Figs. 6–8. One mode can occur in two variations and is for the sake of clearness displayed in Fig. 7(a) and (b).

The description of half cycles is allowed here due to the generation, if properly controlled, of symmetrically shaped full cycles, as they are inherent to the converter's principal structure and method of operation. All of the graphs, except that of Fig. 8, incorporate TLO waveforms. It is noted that in addition to the current i_1, the magnetizing current i_m has also been plotted in the graphs of Figs. 4–8. The four modes which occur are dependent on: the conversion ratio $q = U_o/E_s$, the ratio of the series and magnetizing inductance $\lambda = L_1/L_m$.

As a result of the mathematical analysis given in the appendix, the domain of existence in the conversion ratio

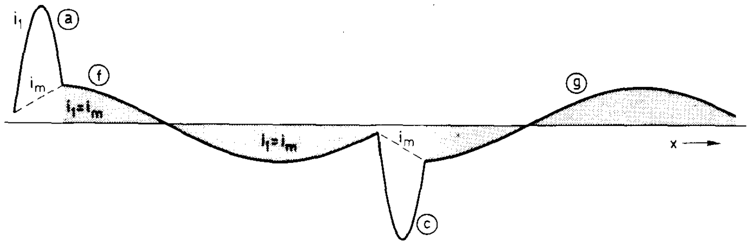

(a)

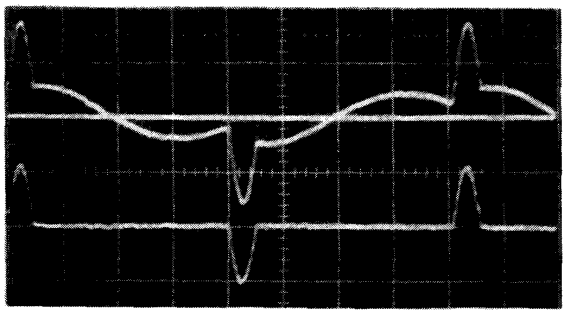

(b)

Fig. 4. (a) Full cycle of resonant current i_1 and magnetizing current i_m, including TLO sine wave segments generated in continuous mode of operation. (b) Experimental waveform ($q = 0.87$; $\lambda = 0.048$): upper trace: resonant current i_1 [20 A/div, 20 μs/div]; lower trace: associated secondary circuit current i_2 [6.5 A/div].

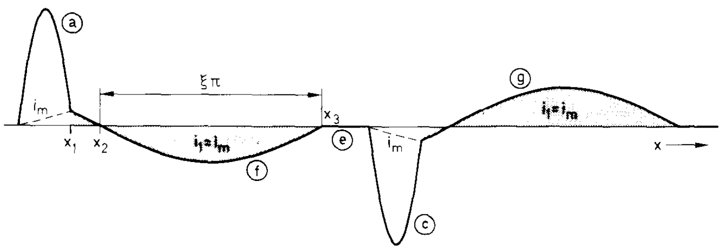

(a)

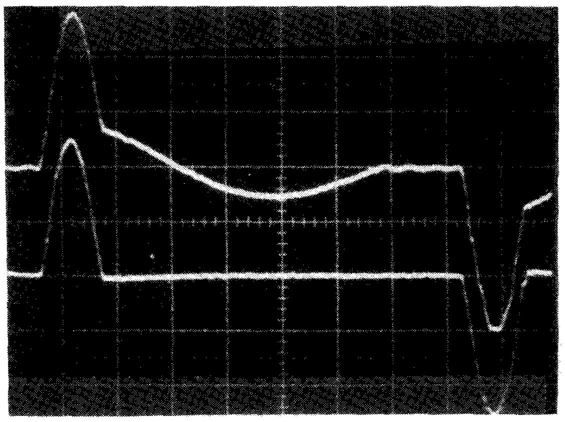

(b)

Fig. 5. (a) Full cycle of resonant current i_1 and magnetizing current i_m, including TLO sine wave segments (length $> \xi\pi$) generated in discontinuous mode of operation. Domain of existence $0.5 + 0.37\lambda < q < 1 - (\pi/2)\sqrt{\lambda}$; $\lambda \ll 1$. (b) Experimental waveform ($q = 0.65$; $\lambda = 0.15$): upper trace: resonant current i_1 [10 A/div, 10 μs/div], lower trace: associated secondary circuit current i_2 [3.3 A/div].

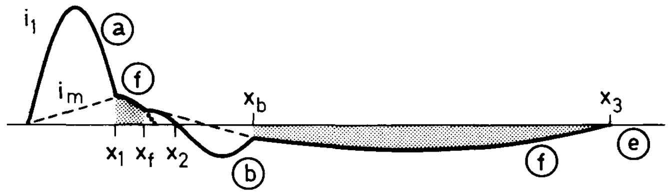

(a)

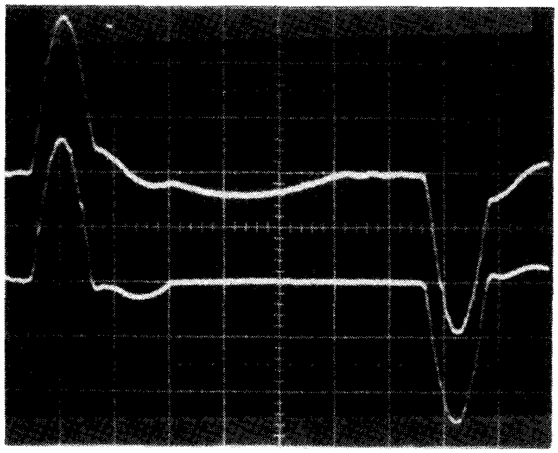

(b)

Fig. 6. (a) Half cycle of resonant current i_1 and magnetizing current i_m, including two TLO sine wave segments generated in discontinuous mode of operation. Domain of existence $0.5 + 0.21\lambda < q < 0.5 + 0.37\lambda$; $\lambda << 1$. (b) Experimental waveform ($q = 0.57$; $\lambda = 0.15$): upper trace: resonant current i_1 [10 A/div, 10 μs/div], lower trace: associated secondary circuit current i_2 [3.3 A/div].

$q = q(\lambda)$, with $\lambda << 1$, has been mentioned in the subtitles of the Figs. 5–8.

The theoretical results are confirmed by experimentally observed waveforms obtained from a dc-dc converter equipped with a step-up transformer (1 : 3) with variable airgap.

The observations are displayed in Figs. 4–8 in accordance with their theoretical counterparts in Figs. 4–8. Further information about the experimental converter are tabulated in Table I below. The moment of firing the switching pair Th11, Th22 is chosen as the starting point for the description of the half cycle. This means that the first sine wave segment of a resonant current half-cycle is generated by the network configuration a of Fig. 3. Or in other words, the first segment of a half cycle of the resonant current consists of the solution of the set relations (2) for $j = k = 1$, and the initial conditions $i_1(0) = 0$ and given $u_{C1}(0)$. During the generation of the first current segment the magnetizing current $i_m(x)$ will increase linearly in time until the moment $x = x_1$, where $i_m(x_1) = i_1(x_1)$ (see the graphs of Figs. 5–8). At time $x = x_1$ the generation of the current i_1 is switched from network configuration a to the one of configurations b or f. The former will be the case if the inequality

$$[E_s - u_{C1}(x_1)]/[1 + \lambda] < -U_o \qquad (7)$$

TABLE I

P_{omax}	200 W	
E_s	24 V	
C_1	5 μF	
L_1	2 μH	
L_m	$\approx$ 42 μH	Fig. 4(b)
L_m	$\approx$ 13 μH	Figs. 5(b), 6(b), 7(c)–(d), 8(b)

holds, and if not, then the latter, switching to f will take place. It is noted that the term $[E_s - u_{C1}(x)]/[1 + \lambda]$ represents the voltage $u_p(x)$ on the primary winding in case that the secondary transformer circuits were to be broken.

Needless to say that, the secondary circuit can only be interrupted at the moment that the current $i_2 = i_1 - i_m$ crosses zero.

Next we consider the case in which the second segment of a half cycle of the resonant current is generated for configuration f (see the graphs of Figs. 5 and 6).

During the generation of the resonant current i_1 in this network, the voltage u_p over the primary windings will be proportional to the slope of the current i_1. Because of this the voltage $[E_s - u_{C1}(x)]/[1 + \lambda]$ will become more negative when x is increased from x_1 to x_2, where x_2 stands for the moment the resonant current i_1 crosses zero.

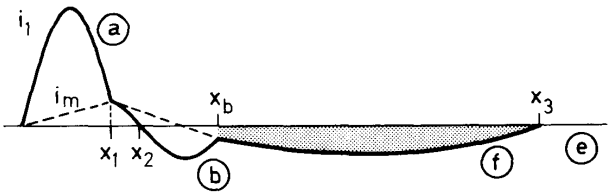

(a)

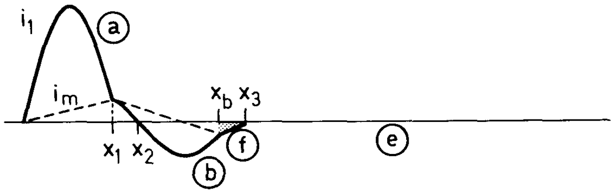

(b)

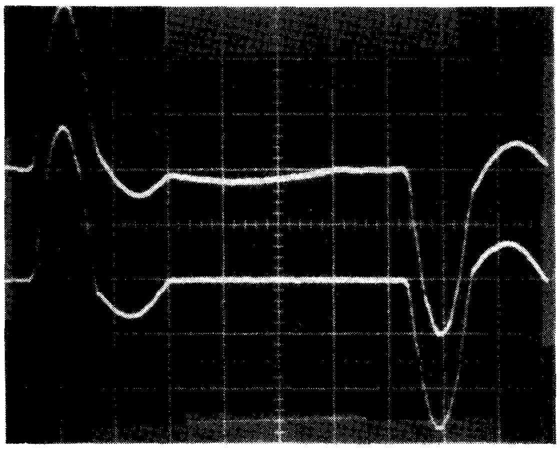

(c)

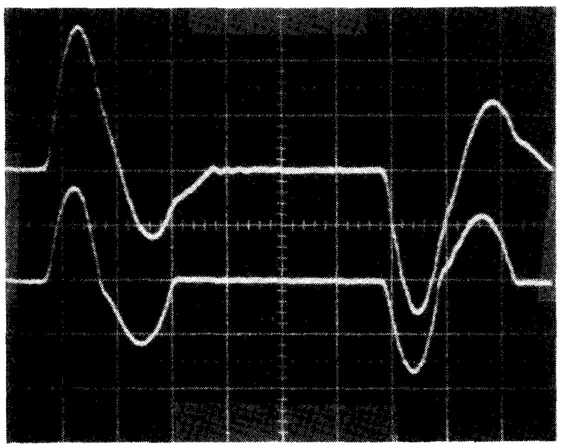

(d)

Fig. 7. (a) Half cycle of resonant current i_1 and magnetizing current i_m, including one TLO sine wave segments of more than $\xi\pi/2$ length, generated in discontinuous mode of operation. Domain of existence $0.5 < q < 0.5 + 0.21\lambda$; $\lambda \ll 1$. (b) Half cycle of resonant current i_1 and magnetizing current i_m, including one TLO sine wave segments of less than $\xi\pi/2$ length, generated in discontinuous mode of operation. Domain of existence: $(3 - \lambda)/9 < q < 0.5$; $\lambda \ll 1$. (c) Experimental waveform ($q = 0.5$; $\lambda = 0.15$): upper trace: resonant current i_1 [10 A/div, 10 μs/div]; lower trace: associated secondary circuit current i_2 [3.3 A/div]. (d) Experimental waveform ($q = 0.35$; $\lambda = 0.15$): upper trace: resonant current i_1 [10 A/div, 10 μs/div]; lower trace: associated secondary circuit current i_2 [3.3 A/div].

As a consequence it can happen that at a certain time $x = x_f$ ($x_1 < x_f < x_2$) the voltage

$$[E_s - u_{C1}(x_f)]/[1 + \lambda] = -U_o. \tag{8}$$

If this equality holds, the generation of current i_1 will be switched at time $x = x_f$ from network f to network b (see Fig. 6).

If the voltage $[E_s - u_{C1}(x)]/[1 + \lambda]$ remains above $-U_o$ during the period $x_1 < x < x_2$, the inequality

$$-U_o < [E_s - u_{C1}(x)]/[1 + \lambda] < U_o \tag{9}$$

will hold for $x > x_2$ up to the end of the half cycle of the resonant current i_1. This implies that the generation of current i_1 will be continued by network f until the moment $x = x_3$, where the antiparallel diodes $D11$ and $D22$ have come out of conduction (see Fig. 5).

Returning to the case in which the generation of current i_1 is switched at time $x = x_f$ to network b, it is obvious that the current i_m will decrease linearly in time for $x > x_f$ until the moment $x = x_b$ where $i_m(x_b)$ equals $i_1(x_b)$, as shown in Fig. 6.

On account of the equality (8) $[E_s - u_{C1}(x_f)]/[1 + \lambda] = -U_o$, it can be demonstrated (see Appendix) that at $x = x_b$ the voltage $[E_s - u_{C1}(x)]/[1 + \lambda] < 0$ and that the inequality

$$-U_o < [E_s - u_{C1}(x)]/[1 + \lambda] < U_o \tag{10}$$

will hold, varying x from x_b up x_3, which is the end of the half cycle of the resonant current i_1.

This implies that at $x = x_b$ the generation of the fourth segment of a half cycle of the resonant current is started by switching from network configuration b to network

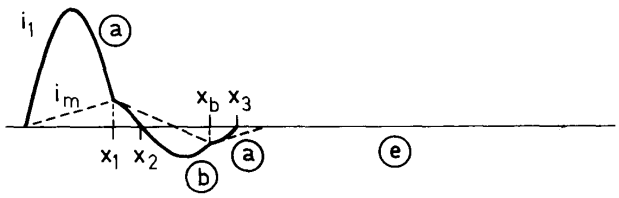

(a)

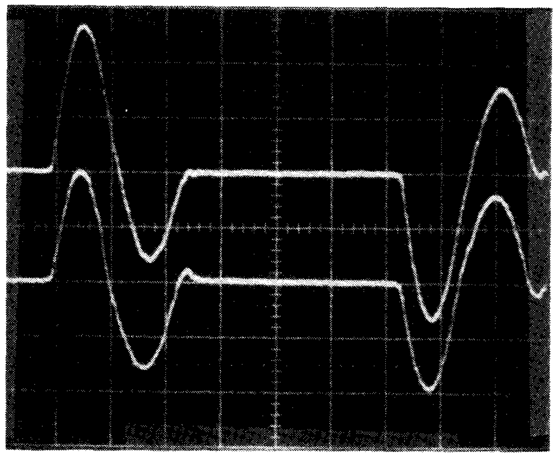

(b)

Fig. 8. (a) Half cycle of resonant current i_1 and magnetizing current i_m, including no TLO sine wave segments, generated in discontinuous mode of operation. Domain of existence: $q < (3 - \lambda)/9$; $\lambda << 1$. (b) Experimental waveform ($q = 0.2$; $\lambda = 0.15$): upper trace: resonant current i_1 [10 A/div, 10 μs/div]; lower trace: associated secondary circuit current i_2 [3.3 A/div].

configuration f. It further implies that this fourth segment, starting with a negative slope, will extend as a sine wave over more than a quarter of a period, up to the moment $x = x_3$ where the antiparallel diodes $D11$ and $D12$ have become nonconducting.

Going back to the case in which the generation of the resonant current is switched at time $x = x_1$ from network configuration a to network configuration b, it is evident that the current i_m will decrease linearly in time for $x > x_1$ until the moment $x = x_b$ where $i_m(x_b)$ equals $i_1(x_b)$ as graphed in Figs. 7(a)–8. At time $x = x_b$ the following can occur: if

$$[E_s - u_{C1}(x_b)]/[1 + \lambda] < U_o \tag{11}$$

then the third sine wave segment will be generated by network f. This segment will extend over more or less than a quarter of a period according to whether the voltage $[E_s - u_{C1}(x_b)]$ has respectively a negative or positive value (see Fig. 7(a) and (b)). If

$$[E_s - u_{C1}(x_b)]/[1 + \lambda] > U_o \tag{12}$$

then the third sine wave segment will be generated by network a (see Fig. 8) which also illustrates the rise of current i_m for $x > x_b$ up to the moment x_4 where i_m becomes zero.

Note that the inequality $i_1(x) > i_m(x)$ must hold for $x_b < x < x_4$, otherwise the secondary current $i_2(x)$ couldn't be positive and as a consequence the magnetizing current $i_m(x)$ wouldn't be increasing for that time interval.

Configurations that represent modes of continuous current operation can be derived from the configurations represented in Figs. 5–8, by eliminating the zero current segment and shifting the remaining half cycles into each other over a certain time distance, say Δx. It is obvious that the occurrence of a certain mode of continuous current operation will depend on the variables q, λ and Δx.

The mathematical details of continuous modes of operation are not explained in this article.

Conclusion

The integration of a power transformer in a series-resonant converter may lead to additional low-frequency oscillations to the basic high-frequency series-resonant phenomena.

The analyses presented classifies TLO waveforms in different modes of operation (see the graphs of Figs. 4–8). The conditions of existence in the conversion ratio $q = q(\lambda)$, with $\lambda << 1$, as calculated in first order approximation in the Appendix, are reported in the subtitles of figures 5 through 8. The theoretical results are in agreement with the experimental observations (see Figs. 5(b), 6(b), 7(c), 7(d), and 8(b).

The amplitude ranges of the TLO waveform segments for the various modes of operation, are easily derivable from the appropriate relations $A25$, $A49$, $A62$, and $A64$, mentioned in the appendix. These ranges of amplitude are

TABLE II

Mode of Operation Presented in	Range of Amplitude of TLO Waveforms
Fig. 5	$\pi E_s \sqrt{\lambda}/(\xi Z_1)$ to $(0.5 + 0.87\lambda)E_s/(\xi Z_1)$
Fig. 6(b)	$(0.5 + 0.87\lambda)E_s/(\xi Z_1)$ to $(0.5 - 1.14\lambda)E_s/(/\xi Z_1)$
Fig. 7(a)	$(0.5 - 1.14\lambda)E_s/(\xi Z_1)$ to zero
Fig. 7(b)	zero to $(3 + 2\lambda)E_s/(9\xi Z_1)$

TABLE III

Mode of Operation Presented in	Condition of Existence
Fig. 5	$0.5 < q < 1$
Fig. 7(a)	$q = 0.5$
Fig. 7(b)	$0.33 < q < 0.5$
Fig. 8	$q < 0.33$

tabulated in Table II. In case the value of λ tends to zero and assuming that ideal switches are applied, the TLO's will tend theoretically to zero in amplitude as well as in oscillation frequency while the electrical charge transported by these TLO's generally will not tend to zero.

Semiconductor switches are not ideal, so that strictly speaking the voltage drop over the switches in the model should have to be taken into account. This is indicative that in practice TLO's will not be generated if λ is smaller than a certain threshold value $\lambda_{thr}(\cdots)$ dependent on a number of parameters.

The voltage drop over the switches is one of the most plausible of these parameters.

It is noticed that setting λ to zero reduces the variation in modes of operation and simplifies the description of the conditions of existence as is shown in the Table III.

The exchange of electric energy between the resonant circuit and the source and load during the existence of a TLO will degrade the power capacity of the power converter as designed with a so-called ideal transformer.

The control of the series-resonant converter can be seriously hindered by the generation of TLO's, especially in cases where the output voltage has to follow a varying reference signal. In [4] it is proposed to avoid the long time constant which is characteristic for the TLO, by introducing a bipolar switch to short circuit the primary winding of the transformer. This switch will then be activated during the period in which the TLO waveforms are supposed to be generated.

It is, however preferable to avoid addition of extra components to the power circuit, especially at higher power levels, by means of a proper design of the series-resonant converter and power transformer in order to achieve a low value of the parameter λ.

Nomenclature

C_1	Capacitance value of resonant capacitor.
E_s	DC-source voltage.
I_o	Load current.
i_1	Resonant current.
$\hat{i}_{11}$	Amplitude of first sinewave segment of resonant current i_1 (Figs. 5(a) and 6(a)).
$\hat{i}_{12}$	Amplitude of the second sinewave segment of resonant current i_1 (Figs. 5(a) and 6(a)).
$\hat{i}_{13}$	Amplitude of third sinewave segment of the resonant current i_1 (Fig. 7(a) and 7(b)).
i_2	Current in secondary windings of the transformer.
i_m	Magnetizing current.
j, k	Pair of ternary variables in expression (2).
L_1	Inductance value of resonant inductor.
L_m	Inductance value of the transformer's magnetizing inductance.
N_1	Number of primary turns.
N_2	Number of secondary turns.
q	Conversion ratio $(N_1/N_2)(U_o/E_s)$.
U_o	Load voltage.
U_{omax}	Maximum value of load voltage U_o.
u_{C1}	Resonant capacitor voltage.
u_{L1}	Resonant inductor voltage.
u_p	Voltage over primary windings of transformer.
x	Normalized time $x = \omega_0 t$.
$x_1, x_f, x_2, x_b, x_3, x_4$	Points of normalized time, defined in Figs. 5(a), 6, 7, and 8.
Z_1	Impedance of resonant circuit; $Z_1 = \sqrt{L_1/C_1}$.
α	$\alpha = \pi - x_1$, see Fig. 5(a).
β	$\beta = (x_2 - x_1)/\xi$, see Fig. 5(a).
γ	$\gamma = x_2 - x_1$, see Fig. 7.
δ	$\delta = \pi - (x_b - x_2)$, see Fig. 7(a).
ϵ	$\epsilon = \pi - [(x_3 - x_b)/\xi]$, see Fig. 7(a) and (b).
θ	Mathematical parameter defined in (A29).
λ	Parameter: $\lambda = L_1/L_m$.
ξ	Parameter: $\xi = \omega_o/\omega_m$.
ω_0	Resonant frequency: $\omega_0 = 1/\sqrt{L_1 C_1}$.
ω_m	Frequency of TLO: $\omega_m = 1/\sqrt{(L_1 + L_m)C_1}$.

Appendix

Mathematical Analysis of Modes of Operation: For simplicity of analysis and presentation the following remarks can be made: (a) the source voltage E_s is set to the value of 1 V without affecting the generality of this analysis, (b) the modes of operation as presented in Figs. 5–8 will be referred to respectively as modes I through IV for the sake of brevity.

Mode of Operation I: From the half cycle as displayed in Fig. 5 the following relations are formulated:

$$i_m(x_1) = i_1(x_1) = \hat{i}_{11} \sin(\alpha) \tag{A1}$$

$$i_m(x_1) = (U_o x)/(\omega_0 L_m)|_0^{x_1} = q(\pi - \alpha)/(\omega_0 L_m). \quad \text{(A2)}$$

Combining (A1) and (A2) gives

$$Z_1\hat{i}_{11} \sin(\alpha) = q(\pi - \alpha)L_1/L_m \text{ or}$$
$$Z_1\hat{i}_{11} \sin(\alpha) = \lambda q(\pi - \alpha). \quad \text{(A3)}$$

Further, can be found

$$\hat{i}_{11} \sin(x_1) = \hat{i}_{12} \sin[x_1/\xi - (x_2/\xi - \pi)], \text{ or}$$
$$\hat{i}_{11} \sin(\alpha) = \hat{i}_{12} \sin(\beta). \quad \text{(A4)}$$

The term $(x_2/\xi - \pi)$ represents here the phase of the second sine wave segment with respect to $x = 0$. From the set of relations (2) the following can be derived:

$$u_{L1}(0^+) = 1 - u_{C1}(0) - q \quad \text{(A5)}$$
$$u_{L1}(x^-) = 1 - u_{C1}(x_1) - q \quad \text{(A6)}$$
$$u_{L1}(x_1^+) + u_p(x_1^+) = (1 + L_m/L_1)u_{L1}(x_1^+) = 1 - u_{C1}(x_1) \quad \text{(A7)}$$
$$u_{L1}(x_3^-) + u_p(x_3^-) = (1 + L_m/L_1)u_{L1}(x_3^-) = 1 - u_{C1}(x_3). \quad \text{(A8)}$$

From the cycle, symmetry can be found:

$$u_{C1}(0) = -u_{C1}(x_3) \quad \text{(A9)}$$

Further it can be written that:

$$u_{L1}(0^+) = L_1\left[\frac{di_1}{dx}\right]\left[\frac{dx}{dt}\right]\Big|_{x\downarrow 0} = \omega_0 L_1\hat{i}_{11} \cos(0) = Z_1\hat{i}_{11} \quad \text{(A10)}$$

$$u_{L1}(x_1^-) = L_1\left[\frac{di_1}{dx}\right]\left[\frac{dx}{dt}\right]\Big|_{x\uparrow x_1} = \omega_0 L_1\hat{i}_{11} \cos(\pi - \alpha) = -Z_1\hat{i}_{11} \cos(\alpha) \quad \text{(A11)}$$

$$u_{L1}(x_1^+) = L_1\left[\frac{di_1}{dx}\right]\left[\frac{dx}{dt}\right]\Big|_{x\downarrow x_1} = (\omega_0 L_1/\xi)\hat{i}_{12} \cos[x_1/\xi - (x_2/\xi - \pi)] = -(Z_1/\xi)\hat{i}_{12} \cos(\beta) \quad \text{(A12)}$$

$$u_{L1}(x_3^-) = L_1\left[\frac{di_1}{dx}\right]\left[\frac{dx}{dt}\right]\Big|_{x\uparrow x_3} = (\omega_0 L_1/\xi)\hat{i}_{12} \cos(0) = Z_1\hat{i}_{12}/\xi. \quad \text{(A13)}$$

Substitution of (A10) in (A5) gives

$$Z_1\hat{i}_{11} = 1 - u_{C1}(0) - q \quad \text{(A14)}$$

Elimination of $u_{L1}(x_1^-)$, $u_{L1}(x_1^+)$ and $u_{C1}(x_1)$ from the relations (A6), (A7), (A11) and (A12) results in

$$-Z_1\hat{i}_{11} \cos(\alpha) + q = -(1 + L_m/L_1)(Z_1/\xi)\hat{i}_{12} \cos(\beta),$$

or

$$Z_1\hat{i}_{11} \cos(\alpha) - q = \xi Z_1\hat{i}_{12} \cos(\beta) \quad \text{(A15)}$$

Elimination of $u_{L1}(x_3^-)$ and $u_{C1}(x_3)$ from (A8), A(9) and (A13) leads to:

$$(1 + L_m/L_1)Z_1\hat{i}_{12}/\xi = 1 + u_{C1}(0)$$

or,

$$\xi Z_1\hat{i}_{12} = 1 + u_{C1}(0). \quad \text{(A16)}$$

Elimination of the terms sin (β) and cos (β) from (A4) and (A15) leads to

$$q^2 - 2qZ_1\hat{i}_{11} \cos(\alpha) + Z_1^2\hat{i}_{11}^2 + (\xi^2 - 1)Z_1^2\hat{i}_{11}^2 \sin^2(\alpha) = \xi^2 Z_1^2\hat{i}_{12}^2. \quad \text{(A17)}$$

Eliminating $u_{C1}(0)$ from (A14) and (A16) results in

$$\xi Z_1\hat{i}_{12} = 2 - Z_1\hat{i}_{11} - q. \quad \text{(A18)}$$

Substitution of (A18) in (A17) and writing $(\xi^2 - 1)$ as $1/\lambda$ gives:

$$4(1 - q) - 2Z_1\hat{i}_{11}[2 - q - q\cos\alpha] = (\hat{i}_{11}^2 Z_1^2/\lambda) \sin^2(\alpha). \quad \text{(A19)}$$

Elimination of $Z_1\hat{i}_{11}$ by substitution of (A3) in (A19) results finally in

$$4(1 - q)\sin\alpha = 2q\lambda(\pi - \alpha)[2 - q - q\cos\alpha] + q^2\lambda(\pi - \alpha)^2 \sin\alpha \quad \text{(A20)}$$

It has already been demonstrated that the existence of mode I requires the validity of the inequality

$$0 > [1 - u_{C1}(x_2)]/[1 + \lambda] > -q. \quad \text{(A21)}$$

Note that if this inequality is transformed into the equality

$$[1 - u_{C1}(x_2)] = -(1 + \lambda)q \quad \text{(A21a)}$$

it determines the limit case in which mode I changes over to mode II. As can be seen from (2), the voltage $[1 - u_{C1}(x_2)]/[1 + \lambda]$ is equivalent to

$$L_m\left[\frac{di_1}{dx}\right]\left[\frac{dx}{dt}\right]\Big|_{x = x_2} = -(\omega_0 L_m/\xi)\hat{i}_{12} \cos(\pi) = -Z_1\hat{i}_{12}/(\xi\lambda). \quad \text{(A21b)}$$

This means that (A21) can be reformulated as

$$Z_1\hat{i}_{12}/(\lambda\xi) < q. \quad \text{(A22)}$$

In the following the angle $\alpha = \alpha(\lambda, q)$ will be approximated from (A20), after which, via (A3) and (A18) the amplitude $\hat{i}_{12} = \hat{i}_{12}(\lambda, q)$ can be obtained in order to put the inequality (A22) solely in λ and q, which determines the domain of existence of mode I. For small values of λ

relation (A20) can be rewritten in second-order approximation as

$$4(1-q)\alpha = 4q\lambda(\pi-\alpha)(1-q) + q^2\lambda\pi^2\alpha$$

or,

$$\alpha = \lambda q\pi/[1-\lambda\{q^2\pi^2/4(1-q)-q\}]. \tag{A23}$$

Substitution of (A23) in (A3) after replacing $\sin\alpha$ by α leads to

$$Z_1\hat{i}_{11} = 1 - \lambda q^2\pi^2/4(1-q). \tag{A24}$$

Substitution of (A24) in (A18) results in

$$\xi Z_1\hat{i}_{12} = 1 - q + \lambda q^2\pi^2/4(1-q). \tag{A25}$$

After substituting (A25) in the inequality (A22) and after recalling that $\lambda\xi^2 = (1+\lambda)$, one obtains

$$1 - q + \lambda q^2\pi^2/4(1-q) < q(\lambda+1). \tag{A26}$$

With algebraic assistance (A27) can be approximated for $\lambda << 1$ as

$$[q - \{0.5 + \lambda(\pi^2/16 - 0.25)\}] \cdot [q - (1 - 0.25\lambda\pi^2)] < 0$$

or

$$[q - (0.5 + 0.37\lambda)][q - (1 - 2.47\lambda)] < 0. \tag{A27}$$

From the last expression one might incorrectly conclude $0.5 + 0.37\lambda + q < 1 - 2.47\lambda$. The right hand bound however has to be chosen smaller, in order to maintain the significance of the relations (A23), (A24) and (A25). Some additional analysis, involving the relations (A3), (A4), (A15), (A16) and $\lambda << 1$, allows one to see that $q = 1 - (\pi/2)\sqrt{\lambda}$ leads to a workable righthand bound corresponding to $\beta = \pi/2$.

This proposed bound taken together with the lefthand bound, already found in (A27), forms the domain of existence of mode I, calculated for $\lambda << 1$,

$$0.5 + 0.37\lambda < q < 1 - (\pi/2)\sqrt{\lambda}. \tag{A28}$$

Mode of Operation II: The boundaries of the domain of existence of mode II are equal to the adjacent domain boundaries of the neighboring modes.

So the right domain boundary of mode II can be set to $q = 0.5 + 0.37\lambda$. The left boundary will be obtained after determination of the domain of mode III, given below:

Mode of Operation III: Consider the relation

$$[1 - u_{C1}(x_1)] = -q - \theta\lambda q. \tag{A29}$$

For $\theta = 1$, this relation will be equivalent to $[1 - u_{C1}(x_1)]/[1+\lambda] = -q$, holding for the limit case that mode II changes over to mode III or vice versa. Likewise one can see that for $\theta < 1$, respectively $\theta > 1$, relation (A29) will hold for cycles generated in mode II and mode III. The set of relations (2) applied to mode III yield the following:

$$u_{L1}(x_1^+) = [1 - u_{C1}(x_1)] + q \tag{A30}$$

$$u_{L1}(x_1^+) = L_1\left[\frac{di_1(x)}{dx}\right]\left[\frac{dx}{dt}\right]\Bigg|_{x\downarrow x_1} = \omega_0 L_1[\hat{i}_{12}\cos\{x_1 - (x_2 - \pi)\} = -Z_1\hat{i}_{12}\cos(\gamma). \tag{A31}$$

From relations (A29), A(30) and (A31) one obtains:

$$Z_1\hat{i}_{12}\cos(\gamma) = \theta\lambda q \tag{A32}$$

From Fig. 7(a) it can be seen that:

$$\hat{i}_{11}\sin(\alpha) = \hat{i}_{12}\sin(\gamma) \tag{A33}$$

Furthermore we note that the relations (A3), (A6), (A9), (A11), and (A14) also hold with respect to mode III and the variables concerned. From the relations (A6), (A11) and (A29) one obtains

$$Z_1\hat{i}_{11}\cos\alpha = 2q + \theta\lambda q \tag{A34}$$

From (A3) and (A33) follows

$$Z_1\hat{i}_{12}\sin(\gamma) = \lambda q(\pi-\alpha) \text{ or}$$

$$Z_1^2\hat{i}_{12}^2 - Z_1^2\hat{i}_{12}^2\cos^2(\gamma) = \lambda^2 q^2(\pi-\alpha)^2.$$

Substitution of (A32) in the last relation results in

$$Z_1\hat{i}_{12} = \theta\lambda q[\{(\pi-\alpha)^2/\theta^2\} + 1]^{1/2} \tag{A35}$$

$$\cos(\gamma) = [(\pi-\alpha)^2/\theta^2] + 1\}^{-1/2}. \tag{A36}$$

One notes that the right hand members of (A35) and (A36) will rapidly converge to $\theta\lambda q$ and the value one for increasing θ. According to (2) one obtains

$$u_{L1}(x_b^-) = 1 - u_{C1}(x_b) + q \tag{A37}$$

$$u_{L1}(x_b^+) + u_p(x_b^+) = (1 + L_m/L_1)u_{L1}(x_b^+) = 1 - u_{C1}(x_b) \tag{A38}$$

$$u_{L1}(x_3^-) + u_p(x_3^-) = (1 + L_m/L_1)u_{L1}(x_3^-) = 1 - u_{C1}(x_3). \tag{A39}$$

Furthermore we note that

$$u_{L1}(x_b^-) = L_1\left[\frac{di_1}{dx}\right]\left[\frac{dx}{dt}\right]\Bigg|_{x\uparrow x_b} = Z_1\hat{i}_{12}\cos(\delta) \tag{A40}$$

$$u_{L1}(x_b^+) = L_1\left[\frac{di_1}{dx}\right]\left[\frac{dx}{dt}\right]\Bigg|_{x\downarrow x_b} = -[Z_1/\xi]\hat{i}_{12}\cos(\epsilon) \tag{A41}$$

$$u_{L1}(x_3^-) = L_1\left[\frac{di_1}{dx}\right]\left[\frac{dx}{dt}\right]\Bigg|_{x\uparrow x_3} = [Z_1/\xi]\hat{i}_{12}\cos(0). \tag{A42}$$

From relations (A37) and (A40) follows that

$$u_{C1}(x_b) = 1 - Z_1\hat{i}_{12}\cos(\delta) + q. \tag{A43}$$

Combining this last relation with (A38) and (A41) leads to

$$Z_1\hat{i}_{12}\cos(\delta) - q = -(\xi Z_1\hat{i}_{13})\cos(\epsilon). \quad \text{(A44)}$$

A combination of (A39) and (A42) will result in

$$\xi Z_1\hat{i}_{13} = 1 - u_{C1}(x_3). \quad \text{(A45)}$$

From Fig. 7(a) can be seen that

$$\frac{x_1}{\hat{i}_{12}\sin(\tau)} = \frac{[(x_b - x_1) - x_1]}{\hat{i}_{12}\sin(\delta)}$$

or,

$$(\pi - \alpha)\sin(\delta) = [(\pi - x_1) + (x_2 - x_1) + (x_b - x_2 - \pi)]\sin(\gamma) \text{ or,}$$

$$(\pi - \alpha)\sin(\delta) = (\alpha + \gamma - \delta)\sin(\gamma) \quad \text{(A46)}$$

and

$$\hat{i}_{12}\sin(\delta) = \hat{i}_{13}\sin(\epsilon). \quad \text{(A47)}$$

Elimination of the terms $\cos(\epsilon)$ and $\sin(\epsilon)$ from (A44) and (A47), results in

$$q^2 - 2qZ_1\hat{i}_{12}\cos(\delta) + Z_1^2\hat{i}_{12}^2 + (Z_1^2\hat{i}_{12}^2/\lambda)\sin^2(\delta) = \xi^2 Z_1^2\hat{i}_{13}^2. \quad \text{(A48)}$$

For $\theta = 1$, neglecting small values of $\alpha = 0\{\lambda\}$ (where $0\{\ \}$ = order of) one finds successively from (A36) and (A46) the angular values:

$$\lambda = 1.26 \text{ rad}$$

$$\delta = 0.296 \text{ rad.}$$

Substitution of the value found for δ in (A48) and elimination of the term $Z_1\hat{i}_{12}$ from the result making use of (A35) for $\theta = 1$ and neglecting α yields

$$(\xi Z_1\hat{i}_{13})^2 = q^2[\lambda^2(\pi^2 + 1) - 5.37\lambda + 1] \approx q^2(1 - 2.69\lambda)^2$$

or

$$\xi Z_1\hat{i}_{13} \approx (1 - 2{,}69\lambda)q. \quad \text{(A49)}$$

Substitution of (A34) with neglecting α in (A14) yields

$$u_{C1}(0) = 1 - 3q - \theta\lambda q. \quad \text{(A50)}$$

From (A50), (A9), and (A45) is obtained:

$$\xi Z_1\hat{i}_{13}(\theta) = 2 - 3q - \theta\lambda q. \quad \text{(A51)}$$

For $\theta = 1$ the last relation can be combined with (A49) giving the result:

$$2 - 4q + 1.69\lambda q = 0$$

or

$$q = 0.5 + 0.21\lambda. \quad \text{(A52)}$$

This last form describes the left domain boundary of mode II and the right domain boundary of mode III.

In the following it is demonstrated that for increasing values of θ the length of the TLO waveform of mode III will decrease and reach the value $\xi\pi/2$, for $\theta = 1/\lambda$.

Assumed is $\lambda << \theta \leq 0\{1/\lambda\}$; $\lambda << 1$. Under these assumptions, and employing (A3), (A36), and (A46) one can write $\alpha = 0\{\lambda\}$, $\gamma = 0\{1/\theta\}$ and $\delta = 0\{1/\theta^2\}$. This means that the relations (A35) and (A44) respectively can be approximated by

$$Z_1\hat{i}_{12} = \theta\lambda q \quad \text{(A53)}$$

$$Z_1\hat{i}_{12} - q = -\xi Z_1\hat{i}_{13}\cos(\epsilon). \quad \text{(A54)}$$

Combination of these last two relations results in:

$$q - \theta\lambda q = \xi Z_1\hat{i}_{13}\cos(\epsilon) \quad \text{(A55)}$$

Elimination of $\hat{i}_{13}$ from (A55) and (A47) leads to

$$tg\epsilon = [\xi Z_1\hat{i}_{12}/(q - \theta\lambda q)]\sin(\delta). \quad \text{(A56)}$$

Inspecting (A56) one sees that for increasing values of θ up to $1/\lambda$ the values of ϵ will increase to $\pi/2$, for $\theta > 1/\lambda$ the value of ϵ will exceed $\pi/2$. Substitution of $\epsilon = \pi/2$ in (A54) and (A47) and combining the results leads to

$$Z_1\hat{i}_{13} = q\sin(\delta) \text{ or,}$$

$$\xi Z_1\hat{i}_{13} = \xi q\sin(\delta). \quad \text{(A57)}$$

For $\theta\lambda = 1$ the relation (A51) can be combined with (A57) giving the result:

$$\xi q\sin(\delta) = 2 - 4q. \quad \text{(A58)}$$

Because of $\delta = 0\{\lambda^2\}$ and $\xi = 0\{\lambda^{-0.5}\}$, relation (A58) can be written as $2 - 4q = 0\{\lambda^{3/2}\}$ or,

$$q = 1/2 - 0\{\lambda^{3/2}\}. \quad \text{(A59)}$$

This last relation represents the "domain-line" for which the length of the TLO waveform segment of mode III measures $\xi\pi/2$ normalized time units. Remark: additional analyses (not presented here), show that the order-term in (A59) can be specified as $0\{\lambda^{3/2}\} = (\pi/6)\lambda^{3/2}$. It has already been mentioned that the existence of mode IV requires the validity of the inequality

$$[1 - u_{C1}(x_b)]/[1 + \lambda] > q. \quad \text{(A60)}$$

In the limit case where mode III changes over to mode IV and vice versa the inequality is transformed into the equality:

$$[1 - u_{C1}(x_b)]/[1 + \lambda] = q. \quad \text{(A61)}$$

Substitution of (A43) with neglected $\delta = 0\{1/\theta^2\}$ in (A61) results in

$$[Z_1\hat{i}_{12} - q] = (1 + \lambda)q. \quad \text{(A62)}$$

Combination of (A62) and (A53) leads to

$$\theta\lambda q - q = (1 + \lambda)q \quad \text{or} \quad \theta = (2 + \lambda)/\lambda \quad \text{(A63)}$$

Setting $\epsilon = \pi$ in (A54) yields

$$\xi Z_1\hat{i}_{13} = Z_1\hat{i}_{12} - q. \quad \text{(A64)}$$

Combining (A9), (A14), and (A45) leads to

$$Z_1\hat{i}_{11} = 2 - Z_1\hat{i}_{13} - q. \tag{A65}$$

Substitution of (A64) in (A65) yields

$$Z_1\hat{i}_{11} = 2 - Z_1\hat{i}_{12}. \tag{A66}$$

Neglecting α in (A34) and combining the result with (A66) and (A53) leads to

$$1 - q = \theta\lambda q. \tag{A67}$$

Substitution of (A63) in (A67) finally results in $(3 + \lambda)q = 1$ or,

$$q = 1/3 - \lambda/9. \tag{A68}$$

This last form describes the left domain boundary of mode III and the right domain boundary of mode IV.

Acknowledgment

The authors wish to express their gratitude to the members of the Power Electronics Laboratory of the Department of Electrical Engineering, who have contributed to this work. The effort of Mr. Kees Weyermans throughout this work is especially appreciated. The authors wish to thank Mrs. Annett Bosch for the manuscript preparation.

References

[1] F. C. Schwarz, "A method of resonant current pulse modulation for power converters," *IEEE Trans. Ind. Electron. Contr. Instrum.*, vol. 17, No. 3, May 1970, pp. 209–221.

[2] ——, "An improved method of resonant current pulse modulation for power converters," *IEEE Transactions Industrial Electron. Contr. Instrum.*, vol. 23, no. 2, pp. 133–141, 1976.

[3] F. C. Schwarz and J. B. Klaassens, "A controllable secondary multikilowatt dc current source with constant maximum power factor in its three phase supply line," *IEEE Trans. Ind. Electron. Contr. Instrum.*, vol. 23, no. 2, pp. 142–150, May 1976.

[4] R. J. King and T. A. Stuart, "Transformer induced instability of the series resonant converter," *IEEE Trans. Aerosp. Electron. Syst.*, vol. AES-19, no. 3, pp. 474–482, May 1983.

[5] F. C. Schwarz, "Engineering information on an analog signal to discrete time interval converter," NASA CR-134544, 1973.

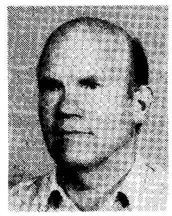

Hans W. Klesser was born in Yogyakarta, Indonesia in 1934. He received the M.S. degree in physics in 1962 from the Delft University of Technology in the Netherlands.

After varied industrial experience he joined the Delft University of Technology in 1970 where he presently is a lecturer in Power Electronics. His reseach interests include: switching power systems, stochastics and control.

J. Ben Klaassens was born in Assen, the Netherlands in 1942. He received the B.S., M.S. and Ph.D. degrees in electrical engineering from the Delft University of Technology in The Netherlands.

He is currently an Associate Professor at the Delft University of Technology teaching graduate courses in the power electronics area. His work has been concerned with inverter circuits, pulsewidth modulation and the control of electrical machinery. His research work and professional publications are in the area of converter systems with high internal pulse frequencies for sub-megawatt power levels employing thyristors and power transistors.

Dr. Klaassens has published a variety of papers on series-resonant converters for low and high power applications. He has designed and built prototypes of the early dc-dc to the recent ac-ac series-resonant converters for a wide variety of applications such as electric motors and generators, communication power supplies, radar signal generators, arc welders and space applications.